Hindawi
International Journal of Aerospace Engineering
Volume 2023, Article ID 8098307, 15 pages
https://doi.org/10.1155/2023/8098307

Research Article

Aerodynamic Interaction Characteristics Study of the Ducted Coaxial Propeller for a Novel eVTOL in Hovering

Junjie Wang[1], **XinFeng Zhang**[1] **and Jiaxin Lu**[2]

[1]*Hangzhou City University, Hangzhou 310015, China*
[2]*Aviation Academy, Nanjing University of Aeronautics and Astronautics, Nanjing 210016, China*

Correspondence should be addressed to XinFeng Zhang; zxf@hzcu.edu.cn

Received 4 November 2022; Revised 25 July 2023; Accepted 1 September 2023; Published 3 October 2023

Academic Editor: Jacopo Serafini

The ducted coaxial propeller (DCP) is highly advantageous in the design of eVTOL aircraft due to its safety, compactness, and low noise levels. To study the aerodynamic characteristics of DCP in hovering, a novel eVTOL was used, and a slip grid model was established to solve the three-dimensional unsteady N-S equation. The aerodynamic characteristics of DCP were compared to those of the free coaxial propeller (FCP) and ducted single propeller (DSP) to reveal the interaction mechanism of unsteady flow between the duct and propellers. The results indicate that the duct significantly mitigates the intensity of tip vortexes by changing the characteristics of propeller tip winding, which reduces the corresponding energy loss. Additionally, the static pressure loss is decreased by the reduced radical-induced velocity in the slipstream area. Finally, the induced power loss is reduced by the decreased axial-induced velocity and suppressed wake contraction, resulting in DCP having 39% higher aerodynamic efficiency than FCP and the duct accounting for 41.7% of the total lift. Although DCP generates 1.77 times more lift than DSP, its aerodynamic efficiency is only 91.08% of DSP.

1. Introduction

The world aviation industry is currently undergoing significant technological changes due to the increasing concerns about low-carbon development. Developing green and efficient urban air transportation will greatly support the efficient operation of the global economy and society [1, 2]. With the advancement of technologies in distributed electric propulsion and motors, electrically driven vertical take-off and landing (eVTOL) aircraft with various configurations are emerging as a sustainable way to address ground transportation in congested metropolitan areas and have become a key development direction for the integration of automotive and aviation industries [3]. Ducted coaxial propeller (DCP), as an innovative form of aviation power device and a representative emerging technology of the aviation power electrification, is designed with a duct surrounding the propellers that makes the safety of the fan more excellent than that of a conventional free coaxial propeller (FCP). Although it reduces the efficiency of the duct in forward flight, it has higher aerodynamic efficiency (lift per power) in hovering and low-speed forward flight, which is more in line with the development goals of green, efficient, safe, and low-noise aviation in the future. Additionally, compared with the ducted single propeller (DSP), the use of an additional propeller and motor in DCP allows for better torque balance and more stable flight and also makes the vehicle more fault-tolerant, thus more reliable and safer [4, 5]. Therefore, DCP has become a popular choice for eVTOL aircraft designed for low-speed flight.

DCP is the key propulsion system of eVOTL aircraft, and it is crucial to study its aerodynamic characteristics. Since the lower propeller of DCP is in the downwash and wake of the upper propeller, the duct suppresses the generation of the tip vortex, and the contraction of the wake of the upper and lower propellers. Therefore, there is complex aerodynamic interference between the duct and the propellers, as well as the upper propeller and the lower propeller. The interaction of propeller tip leakage flow, the boundary layer of the duct's wall, and the propeller wake make the internal flow field of the duct extremely complex. The strong unsteady characteristics increase the difficulty in the

calculation and analysis of the interference mechanisms. In the last century, a lot of theoretical research and practical exploration of ducted-UAV were conducted, and some valuable conclusions were drawn [6, 7]. However, limited by computation technology, the relevant methods mainly relied on experiments and engineering estimation, which inevitably ignored part of the flow field details and interference mechanism. At the beginning of this century, with the growth of interest in UAVs and electric propulsion, more researchers focus on ducted fan aircraft and developer the combination of modern experimental techniques and CFD simulations [8, 9]. The results measured by experimental methods are highly reliable, but the negative factors such as incoming turbulence, experimental errors, and stand interference make it difficult to obtain intuitive flow field information and accurate aerodynamic interference details [10]. CFD methods combine fluid mechanics and numerical computation through computer technology to simulate and analyze fluid problems and visually display their flow fields. Moreover, the cost of CFD calculation is low, and it is easier to predict the noise of the propeller [11, 12]. While they can simulate the details of the flow field, the accuracy of the calculations is questionable, can simulate the flow field details, but the accuracy of calculation is doubtful. The Navier-Stokes (N-S) equation, although it has a large calculation volume, can capture the detailed flow of the propeller and the boundary layer of the duct surface, such as propeller vortex interference [13, 14]. Qing et al. used the CFD method to study the effects of duct shape and propeller torsion angle on the aerodynamic performance of small ducted fans [15, 16]. Shukla et al. adopted a hybrid approach of using both CFD simulations and experimental methods to investigate the aerodynamic interference between duct fans in their research [17–19]. This approach not only enhances the credibility of the study but also provides a comprehensive understanding of the flow field disturbances. However, this type of research has the following shortcomings. Firstly, the related research focuses on DSP UAVs, while there is not much work on the aerodynamic characteristics of the unsteady flow of DCP aircraft. Secondly, the related researches fail to analyze the details and mechanisms of the interference thoroughly. Therefore, the aerodynamic characteristics and interference mechanism of DCP are still unclear, so it is necessary to carry out further research. Finally, most literature focused on small ducted fans, with hardly any research public on large ones used in eVTOL aircraft. The Reynolds number of the latter is greatly different from the former. As a result, the aerodynamic interference performance is different, so there are still many problems that need to be further studied and solved.

This paper is aimed at investigating the aerodynamic interference mechanism within the DCP system for eVTOL aircraft. To achieve this goal, a combination of experimental and CFD methods is used to analyze the unsteady interference among the duct and propellers. By comparing the aerodynamic characteristics of the DCP, DSP, and FCP, the study aims to provide guidance for noise reduction and improvement of aerodynamic performance in eVTOL aircraft applications. Due to the complex aerodynamic interaction between the components within the DCP system, it is difficult to measure the aerodynamic forces of different components separately in experiments. Therefore, a numerical simulation method based on the slip grid model is established to verify the accuracy of the CFD method with experimental data.

This paper is structured as follows: Section 2 describes the numerical simulation method and grid refinement method used in the study and validates the method with experimental data. Section 3 compares the unsteady aerodynamic characteristics of DCP, FCP, and DSP, respectively, and discusses the aerodynamic characteristics of the unsteady flow between the duct and propellers. Finally, Section 4 presents the conclusions of the study.

2. Methodology

2.1. Study Object Description. The overall design of a novel eVTOL aircraft (rendering as Figure 1(a)) is carried out. It contains 4 DCPs with the lift of 3000 N for each, thus reaching a takeoff weight of 1.2 tons [20]. The novel eVTOL aircraft is capable of vertical take-off and landing, as well as independent hovering, and features high efficiency, low noise, and a wide operational range. Its main operating conditions include hovering and forward flight at low speeds. It can be applied in various fields such as urban firefighting, urban air transportation, and tourism. This paper mainly focuses on the aerodynamic interference characteristics of DCP. Figure 1 presents the main aerodynamic parameters of DCP. Propeller parameters can be found in reference [20]. The simplified model consists of an upper propeller, a lower propeller, and a duct. The complete duct structure is shown in Figure 1(b).

In order to analyze the interference characteristics of DCP, it is compared with FCP and DSP, respectively. Compared with DCP, FCP has no duct, and DSP has one less lower propeller, as shown in Figure 2. The other parameters are the same for the three configurations. The aerodynamic interference between the duct and coaxial propellers and the related aerodynamic mechanism of lift increase can be obtained by comparing the aerodynamic characteristics of DCP and FCP. The aerodynamic interference between the duct with one propeller and the other propeller and the related interference mechanism can be obtained by comparing the aerodynamic characteristics of DCP and DSP.

2.2. Numerical Method. The widely applicable and highly functional commercial CFD software Ansys Fluent was used to simulate the flow field of the DCP [21]. In this paper, the RANS (Reynolds Average Navier-Stokes) equations were used to describe the flow characteristics of the viscous fluid. A coupled solver is used to solve the mass, momentum, and energy equations simultaneously, and then the turbulence equation is solved. The equations are as follows [22]:

$$\frac{\partial \rho}{\partial t} + \frac{\partial}{\partial x_i}(\rho u_i) = 0, \tag{1}$$

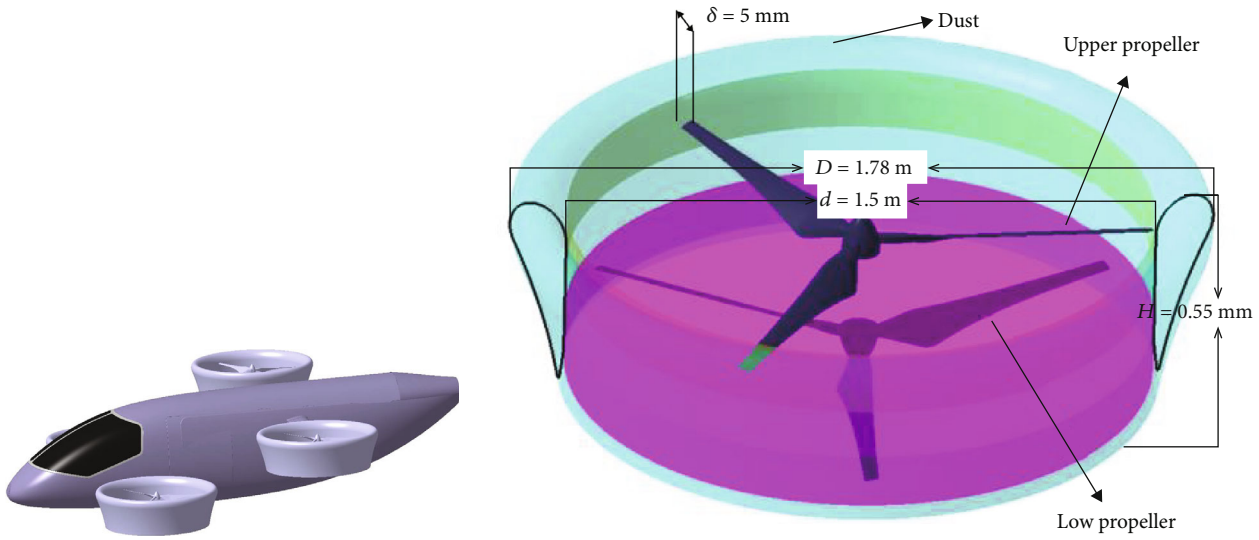

(a) The novel eVTOL aircraft with DCP (b) Parts diagram of DCP

Figure 1: DCP aerodynamic model and parameters [20].

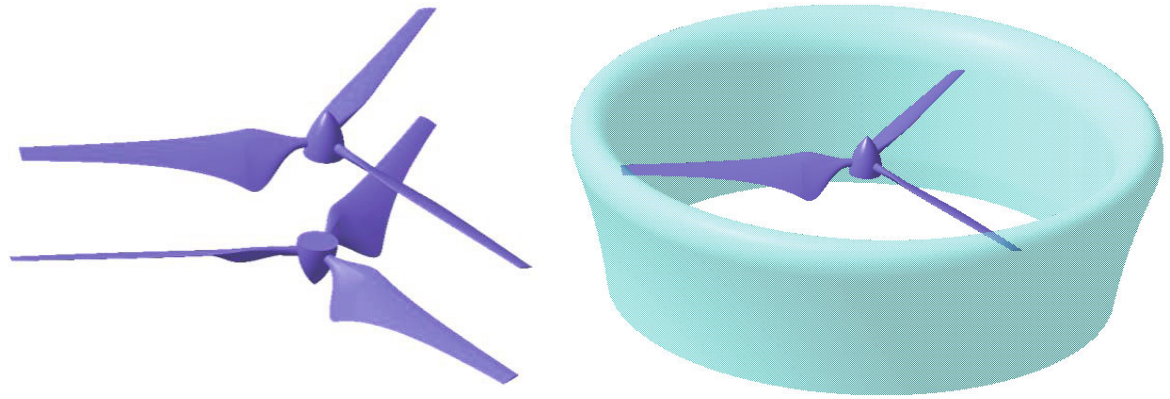

(a) Model of FSP (b) Model of DSP

Figure 2: Model of FSP and DSP.

$$\frac{\partial}{\partial t}(\rho u_i) + \frac{\partial}{\partial x_j}(\rho u_i u_j) = -\frac{\partial \rho}{\partial x_i} + \frac{\partial}{\partial x_j}\left[\mu\left(\frac{\partial u_i}{\partial x_j} + \frac{\partial u_j}{\partial x_i} - \frac{2}{3}\delta_{ij}\frac{\partial u_i}{\partial u_j}\right)\right] + \frac{\partial}{\partial x_j}\left(-\rho\overline{u_i' u_j'}\right). \tag{2}$$

$-\rho\overline{u_i' u_j'}$ is the Reynolds stress component term, which can be written through the vortex viscosity hypothesis proposed by Boussinesq as:

$$-\rho\overline{u_i' u_j'} = \mu_t\left(\frac{\partial u_i}{\partial x_j} + \frac{\partial u_j}{\partial x_i}\right) - \frac{2}{3}\left(\rho k + \mu_t\frac{\partial u_k}{\partial x_k}\right)\delta_{ij} \tag{3}$$

μ_t is the turbulent viscosity, u_i is the time-averaged velocity, and k is the turbulent energy.

Turbulence models can be used to close the fluid flow control equations and are crucial for accurately simulating unsteady and complex flow. In this paper, the k-ω SST (shear stress transport) turbulence model is chosen [23]. To reduce computational costs, the finite volume method with second-order accuracy is used for spatial discretization [24]. The ROE format is used for convective flow calculation, and the approximate Riemann approximation is used to solve the convective flow on the grid boundary [25]. In order to improve the efficiency and accuracy of solving the unsteady flow field, the dual-time implicit LU-SGS iterative method is used for time discretization [26]. The idea is to conduct approximate LDU decomposition on the implicit operator, and the LU-SGS decomposition method avoids matrix inversion by performing two iterative solutions in both the forward and backward directions.

2.3. Grid Refinement. The geometry of the DCP system, particularly in the blade gap area and near the tip region, is complex with duct surfaces and varying pressure gradients due to the presence of shock waves and flow separation.

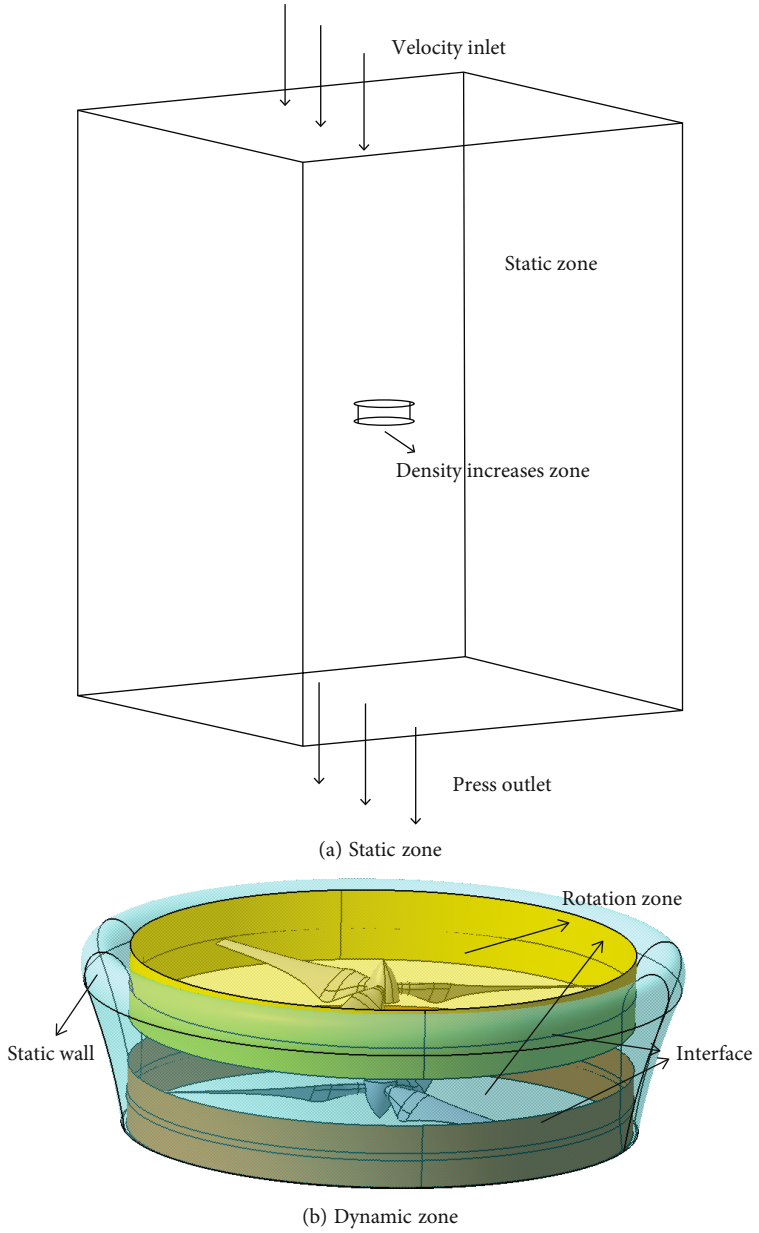

Figure 3: Boundary conditions [20].

To accurately capture the complex flow physics, a non-structured mesh with strong adaptive capabilities was generated using the ICEM program. This type of mesh is good at handling complex geometries, can conform to the shape of the geometry, is flexible in generating meshes, and is not restricted by the topology of mesh nodes, with strong spatial filling capability.

Although a larger computational domain theoretically leads to less interference with the model results, limited computing resources necessitated the use of a rectangular box as the computational domain. The inlet and outlet boundary conditions were set as velocity inlet and pressure outlet, respectively, as shown in Figure 3. The grid around the cylindrical intersection was further refined to improve computational efficiency and simulation resolution. The sliding mesh technique was used to avoid distortion of the boundary layer mesh during mesh movement and improve computational efficiency. The fluid domain was divided into one static and two rotating domains, with the duct located in the static domain. Each rotating zone was enclosed by a cylinder with a volume greater than that of the propeller and within the duct, with the propeller simulated through the sliding mesh technology. The rotating zones were further refined to improve grid quality. A conservative coupling by pitching row was used to connect the different rotating domains to ensure mass, momentum, and energy conservation.

The use of prismatic mesh in the duct and propellers improved the accuracy of the viscous boundary layer mesh and allowed for accurate simulation of the flow velocity and friction drag, resulting in more precise calculation of power. The computational domain was filled with

Table 1: Lift of the DCP with different heights of the first boundary layer.

d_1	Lift (N)	Iteration_error = $L_{Newmesh} - L_{Oldmesh}/L_{Newmesh}$ *100%
0.0001 m	2686	Baseline
0.00005 m	2763	2.78%
0.00003 m	2802	1.4%
0.00001 m	2819	0.6%

Table 2: Lift of the DCP with different mesh density.

Mesh number	Lift(N)	Iteration_error = $L_{Newmesh} - L_{Oldmesh}/L_{Newmesh}$ *100%
100 million	2773	Baseline
140 million (refined in rotation domains)	2802	1.03%
180 million (overall refined)	2818	0.57%
80 million (overall sparse)	2705	3.8%

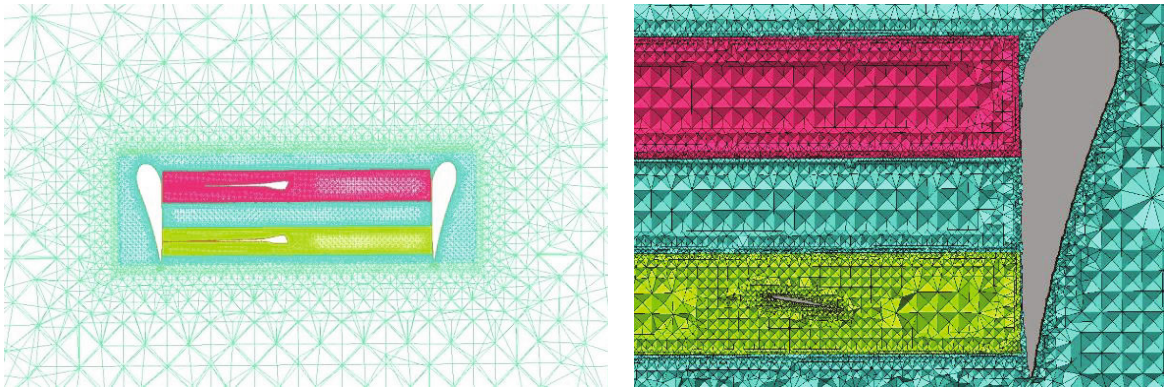

(a) Body grid sections (b) Grid detail of propeller and duct

Figure 4: Grid diagram [20].

tetrahedral meshes, with a boundary layer growth rate of 1.1 and a $y+$ value of 1.

In the mesh irrelevance analysis, taking viscous effects into account, the influence of the height of the first boundary layer mesh of the propeller and the duct as well as mesh density on the calculation results were analyzed separately. To accurately simulate the viscous interaction within the boundary layer, an appropriate boundary layer grid is required for flows with Reynolds numbers ranging from 10^5 to 10^6. In this study, the first boundary layer grid height (d_1) was varied between 0.0001 m, 0.00005 m, 0.00003 m, and 0.00001 m with a growth rate of 1.2 and 12 total layers of the mesh. The total lift of the DCP in hovering was then calculated with both upper and lower propellers operating at 2500 rpm. The mesh irrelevance analysis results, shown in Table 1, indicate that a grid height of 0.00003 m is sufficient for achieving the desired calculation accuracy.

The setting of the grid quantity is a crucial step in determining the grid strategy. The refinement level of the grid affects the simulation results, and setting different grid sizes for different areas can save computational resources while ensuring simulation accuracy. However, once the grid quantity reaches a certain level, the simulation results become less sensitive to changes in the grid quantity. In order to investigate the effect of grid density on the calculation results, the grid density was controlled by adjusting the mesh size of the rotation domains enclosing the propellers and the static domain enclosing the duct. The total number of grid elements used was 6 million (overall sparse), 10 million (baseline), 14 million (refined in rotation domains), and 18 million (overall refined). The total lift of the DCP during hovering was calculated at 2500 RPM for both the upper and lower propellers, and the results are presented in Table 2. It was found that the mesh density of the rotation domains had a significant impact on the calculation results, and a mesh with 14 million elements was chosen to calculate the aerodynamic performance of the model.

Based on the analysis of the grid irrelevance, it has been determined that a grid with 14 million elements and a first boundary layer height of 0.00003 m, as depicted in Figure 4, is appropriate for achieving accurate calculations.

Figure 5: Lift and power measurement test bench [20].

2.4. Method Validation. To establish a reliable and accurate numerical simulation method, a verification process was conducted by comparing simulation results with experimental data. A ground-based performance test of the DCP system was carried out, which included lift and power measurement using a designed DCP lift and power measurement system, as described in reference [20]. The experimental rig is illustrated in Figure 5.

During the experiments, the entire DCP system operated steadily and reliably without any significant anomalies from 500 rpm to 2500 rpm. The ground performance test was carried out to obtain some steady-state performance data of the DCP. Comparison with the experimental data is presented in Figure 6, indicating that the CFD simulation results are consistent with the experimental trends and in good agreement. However, the calculated lift and power values were slightly lower than the experimental values, with errors of less than 5%. Therefore, the CFD method established in this study is suitable for simulating the flow field of the DCP system.

3. Aerodynamic Characteristics Feature and Discussion

3.1. DCP and FCP Comparison. FCP has the advantages of compact structure and power redundancy, so it is widely used in eVTOL aircraft, such as EH216. While DCP has one more duct than FCP, which can effectively improve the lift characteristics [27].

According to Figure 7, compared with FCP, the characteristics of the lift and torque of each component of DCP are as follows. (1) At the same rotational speed, the action of the duct makes the lift of the upper and lower propellers within the duct smaller than that of FCP; that is, the duct will decrease the lift generated by the propellers. The upper propeller in the duct accounts for 75.8% of the propeller lift of FCP, and the lower propeller in the duct accounts for 86.6%. (2) Due to the flow-inducing and contraction effect of the propellers, the winding flow of the duct lip provides additional lift. The duct lift accounts for 41.7% of the total lift of DCP; this value does not change with the variation

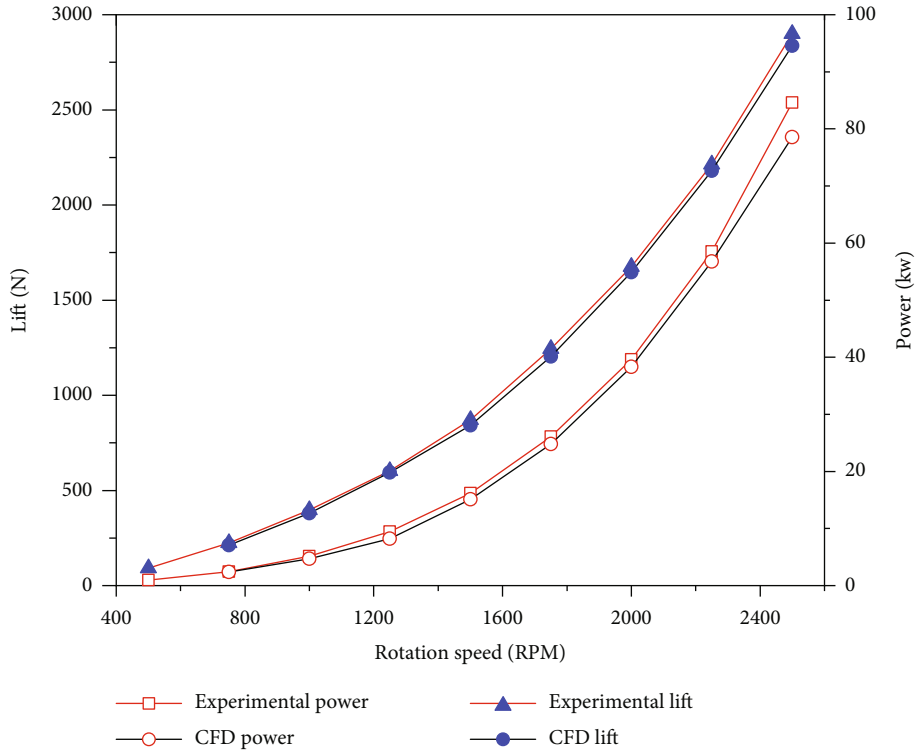

Figure 6: Comparison of CFD calculated values and experimental values [20].

of rotational speed, and it is related to the aerodynamic shape parameters of the duct and propeller. (3) The additional lift of the duct makes the total lift of DCP larger than that of FCP, and the total lift of DCP is 1.39 times that of FCP, but the torque is basically the same. It means the total aerodynamic efficiency of DCP is 1.39 times that of FCP. (4) Due to the interaction between the duct and propeller, the lift generated by the lower propeller is larger than that of the upper propeller; this is the opposite to the characteristic of FCP.

The following analysis focuses on the relevant mechanism from the flow field perspective. Figure 8 shows the streamline diagram and pressure contour of FCP and DCP. Compared with FCP, the characteristics of DCP mainly lie in: (1) at the propeller tip of FCP, the phenomenon of tip vortex flow occurs. The lower propeller produces a larger tip vortex compared with the upper propeller, while there is no significant vortex generated around both the upper and lower propellers for the DCP. Thus, the duct significantly reduces the tip vortex generation and reduces the tip vortex energy loss. (2) FCP has an obvious wake contraction effect. In contrast, the inner wall of the duct suppresses the wake contraction, improving the airflow state under the upper propeller disc in DCP. As a result, the area of downwash is increased and the induced velocity is reduced, which further reduces the induced energy loss of the whole system. (3) The leading edge of the inlet area of the duct produces a large negative pressure zone, while the pressure in the lower half of the outer and inner walls of the duct is larger than the pressure in the negative pressure zone at the leading edge, so the duct produces additional lift. (4) The two propellers of DCP each produce a negative pressure zone above the propellers larger than that of FCP, which produces a smaller high pressure zone, resulting in a smaller total lift generation compared with FCP.

The three-dimensional effect caused by the tip vortex leads to pressure loss at the propeller tip and reduction of effective angle near the tip, reducing the lift-to-drag ratio of the propeller tip. Propeller efficiency depends on the lift direction of blade element, so the reduction of lift to drag ratio will decrease the lift and the FCP aerodynamic efficiency. It can be seen that duct can change propeller tip winding and reduce the strength of tip vortex, which thus reduces the aerodynamic load on the propeller, increases the lift-to-drag ratio of the propeller tip, and improves the aerodynamic efficiency of the propeller tip.

Figure 9 shows the contour of the axial induced velocity of DCP and FCP. It can be seen that the axial airflow acceleration by the upper propeller of DCP is slightly smaller than that of FCP. This is because the duct suppresses the wake contraction, indicating that the duct changes the downwash downstream of the propeller and reduces the slipstream area-induced velocity. From the momentum theorem, it is known that the lift generated by the propeller decreases when the axial induced velocity decreases. The ideal efficiency of propeller is determined by the axial induced power. Axial-induced power loss is the mechanical energy carried by the airflow in the slipstream area of the propeller, which is converted into kinetic energy of the airflow. Therefore, when axial induced velocity decreases, the axial induced power decreases accordingly, and the aerodynamic efficiency of the propeller increases. In FCP, the lower

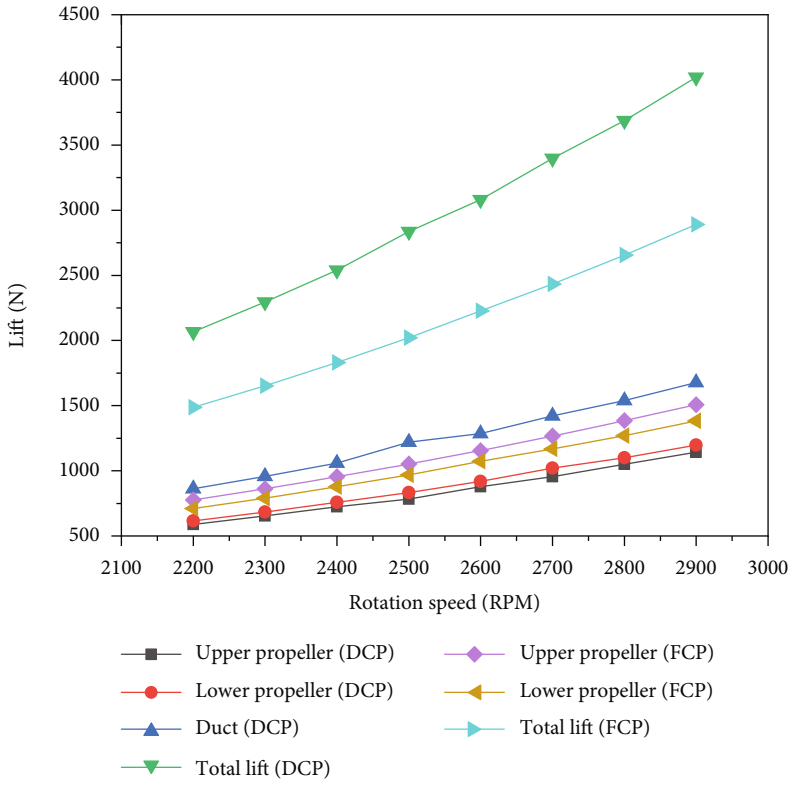

(a) Lift breakdown on each part under different rotation speed

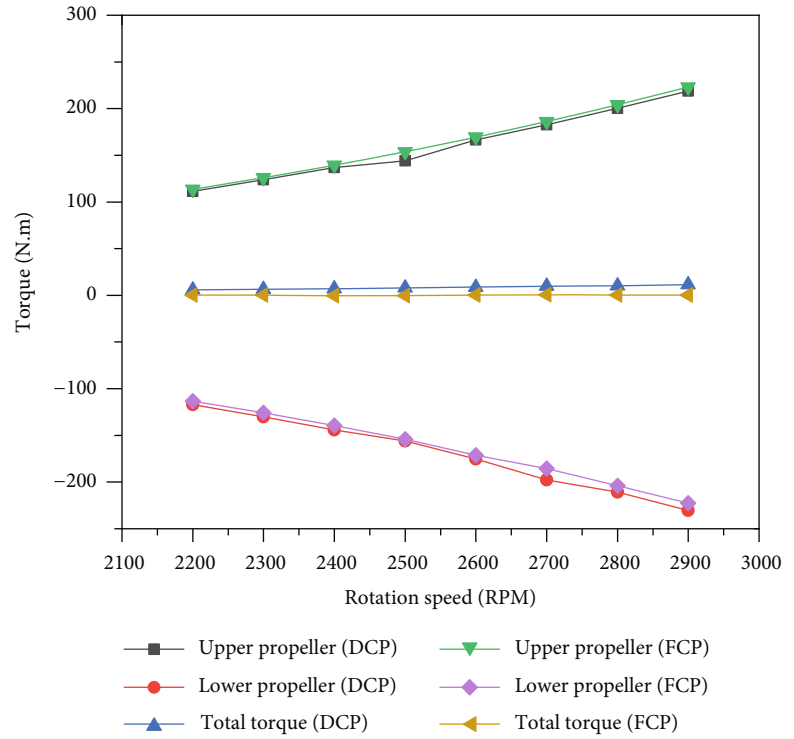

(b) Torque breakdown on each part under different rotation speeds

Figure 7: Lift and torque breakdown on each parts of DCP and FCP.

propeller is subject to the aerodynamic interference of the upper propeller, and the downwash velocity of the lower propeller is larger than that of the upper propeller, so the efficiency is smaller than that of the upper propeller. In contrast, in DCP, the effect of the duct on the propeller downwash makes the lower propeller more efficient. The

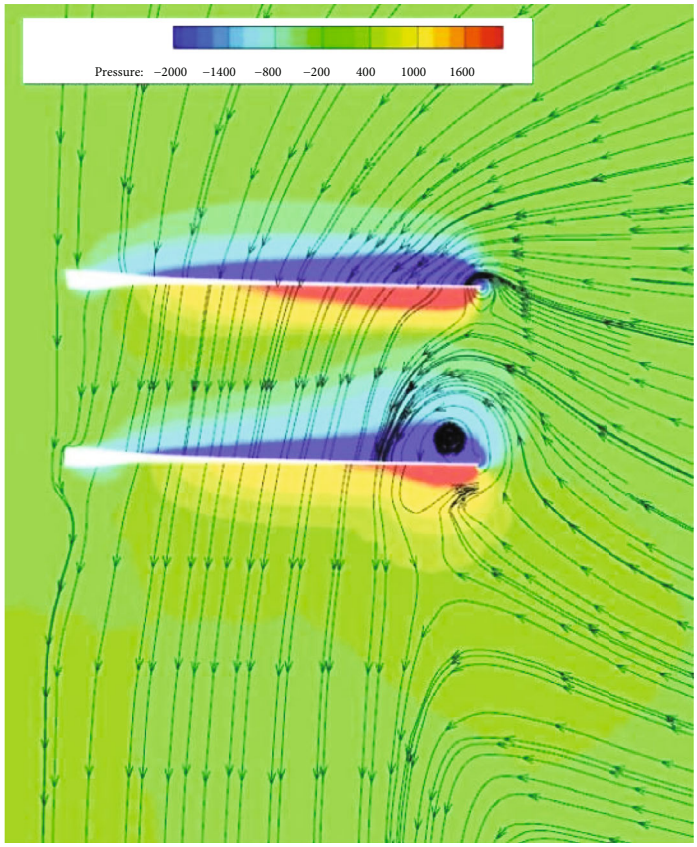

(a) Streamline diagram and pressure contour of FCP

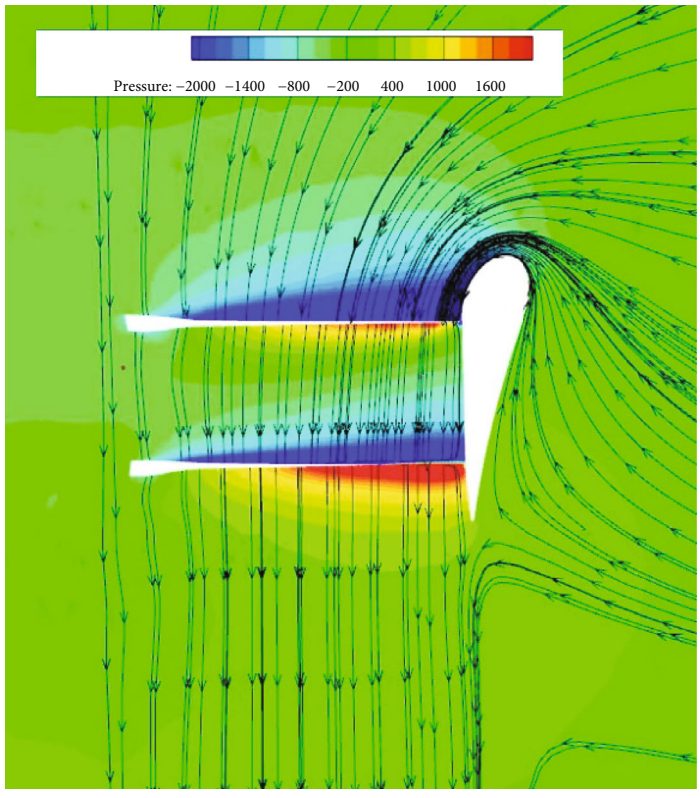

(b) Streamline diagram and pressure contour of DCP

Figure 8: Streamline diagram and pressure contour.

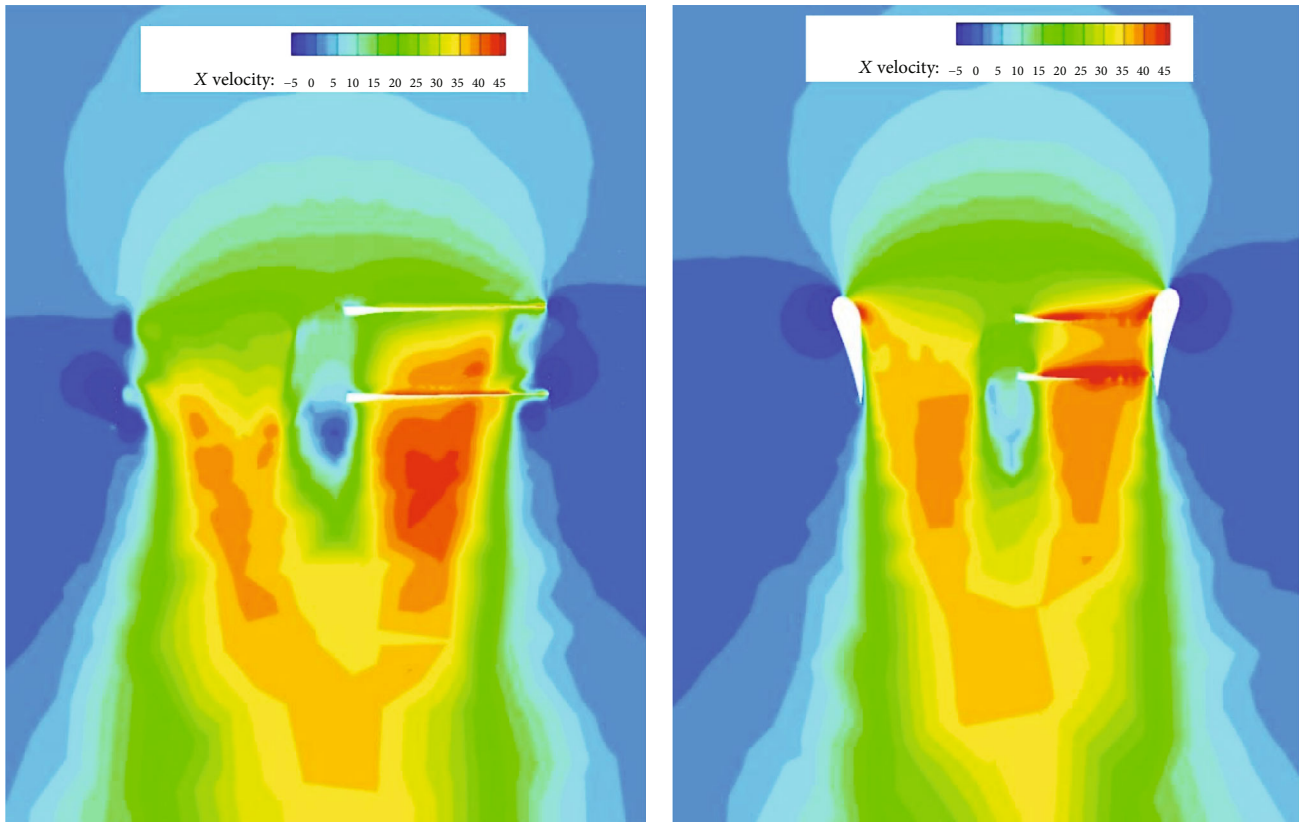

(a) Contour of the axial induced velocity of FCP

(b) Contour of the axial induced velocity of DCP

Figure 9: Contour of axial induced velocity.

downwash velocity of the lower propeller is more or less the same as that of the upper propeller, resulting in the efficiency of the lower propeller being close to that of the upper propeller. Duct brings contradiction to lift and efficiency of the propeller. The downwash kinetic energy loss due to the duct is converted into pressure energy of the duct, which generates additional lift, so the total lift and total aerodynamic efficiency generated by DCP are larger than that of FCP.

Figure 10 shows the streamline diagrams. It can be seen that the upper and lower propellers of DCP and FCP are coaxially reversed, and their streamlines have certain similarities. The spiral of the streamlines below the lower propeller is obviously weakened, but they all show a certain spiral shape, which is due to the existence of radical-induced velocity in the slipstream area due to the rotation of the propeller. Compared with FCP, DCP has relatively smaller twist streamlines, which indicates that the duct has a certain inhibitory effect on the radical-induced velocity of the propeller slipstream area. The formation of radical-induced velocity requires a corresponding centrifugal force on the airflow, which reduces the static pressure in the slipstream area and increases the loss of axial-induced power. This result in less mechanical energy of the propeller converted into pressure energy, making the propeller's aerodynamic efficiency lower. The duct reduces the radical-induced velocity of the propeller, decreasing the static pressure loss in the slipstream area. This is the reason why the static pressure of the slipstream area of FCP is smaller than that of DCP. Since the corresponding energy loss is reduced, the propeller's aerodynamic efficiency is improved.

3.2. DCP and DSP Comparison. DSP has the advantages of high efficiency and low noise [28], making it plays a significant role in eVTOL aircraft application. Compared with DSP, DCP has one more propeller. The coaxial propellers not only make the structure more compact but also make the vehicle safer due to the power redundancy.

Figure 11 shows the lift and torque variations of DCP and DSP. Compared with the DSP, the force and torque characteristics of each DCP component are as follows: (1) At the same rotational speed, the action of the lower propeller increases the airflow speed of the duct lip, so the proportion of lift generated by the duct of the DCP is larger than that of the DSP, where the lift of the duct of the DCP accounts for 41.7% of the total lift and that of the DSP is 37.1%. (2) The total lift of DSP is smaller than that of DCP, but the lift of the propeller in DSP is larger than that of the upper propeller of DCP, while the torque is basically the same, thus the power consumed is almost equal. It reveals that the total aerodynamic efficiency (lift/power) of DSP is larger than that of DCP.

Then the interference mechanism of the propeller on DCP is analyzed from the flow field perspective. Combining

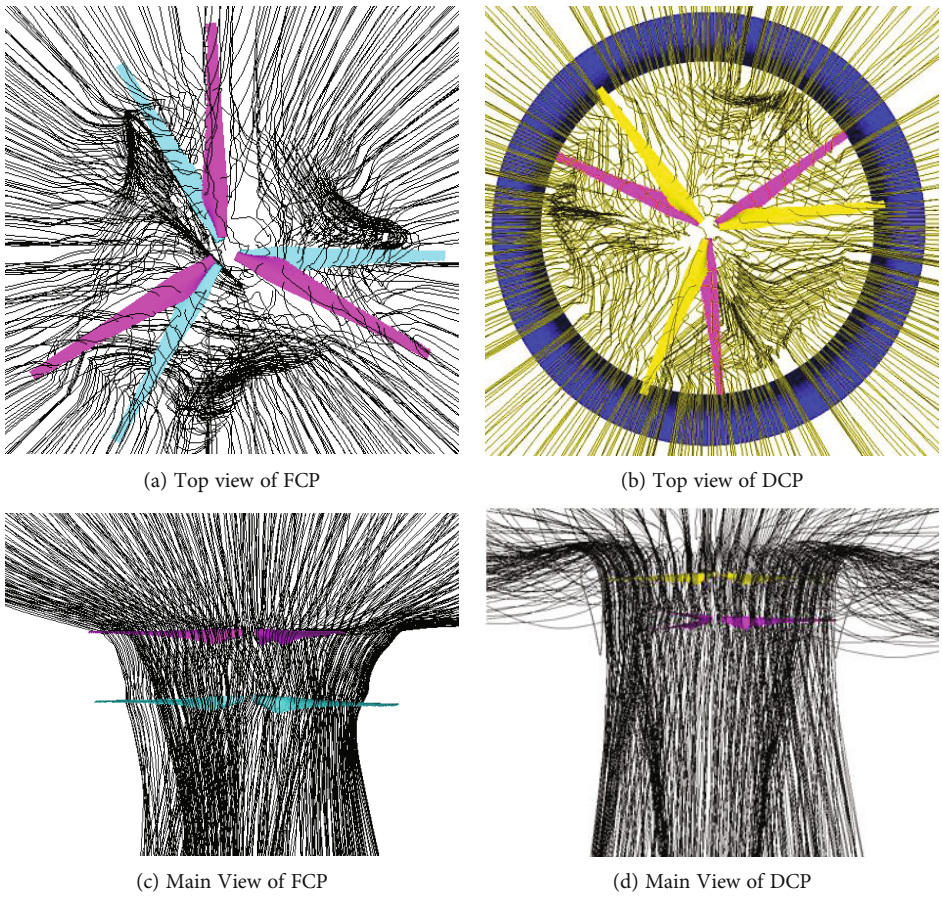

(a) Top view of FCP (b) Top view of DCP

(c) Main View of FCP (d) Main View of DCP

Figure 10: Streamline diagram of FCP and DCP.

Figure 12 with Figures 8(b) and 9(b), it can be seen that the aerodynamic characteristics difference between DCP and DSP mainly lies in (1) DCP has one more co-axial counter propeller based on DSP; the additional lower propeller produces suction effect, increases the inlet air through the duct and the airflow speed at the lip of the duct, and thus increases the lift of the duct. At the same time, the speed of the downwash is increased, which decreases the effective angle of the propeller in the duct, and thus the lift of the propeller is reduced. (2) Although the lift distribution has been changed, the torque magnitude of the upper propeller remains the same, and the aerodynamic efficiency (lift/power) of DSP is larger than that of DCP because the induced velocity and the induced power increase and the overall efficiency decreases. (3) The inner wall of the duct inhibits the wake contraction and improves the state of the airflow below the upper propeller disc in the DCP, which increases the area of the slipstream area and reduces the induced velocity, further reducing the energy loss of the whole system. However, the magnitude of the wake contraction in the DSP is larger than that in the DCP. (4) Compared with the propeller in DSP, the upper propeller in the DCP has a larger negative pressure area above the disc and a lower high-pressure area below the disc, resulting in less lift generated. Unlike the DSP, the lower propeller in the DCP is affected by the upper propeller downwash; the negative pressure area above its disc is significantly smaller than the same part of the upper propeller, and the high-pressure area below the upper propeller disc in the DCP is smaller than the same part of the lower propeller. The high-pressure area below the DCP upper propeller is smaller than the same area of the lower propeller, resulting in the pressure difference between the upper and lower surfaces of the lower propeller being larger than that of the upper propeller. This brings a larger lift to the lower propeller, although the difference is not significant. This phenomenon can be explained as the interference of the upper propeller because of the suction effect of the lower propeller, which makes the lift generated by the upper propeller decrease. Due to the interference of the suction effect of the upper propeller, the lift generated by the lower propeller is increased. (5) The suction effect of the lower propeller changes the downwash state of the propeller, increasing the axial induced velocity, and the lift of both the upper and lower propellers is decreased. On the one hand, it increases the additional lift of the duct; on the other hand, it increases the loss of axial induced power loss and decreases the propeller aerodynamic efficiency. Therefore, the total lift generated by DCP is larger than that of DSP, but the aerodynamic efficiency is not as good as that of DSP.

By comparing Figures 10 and 13, it can be seen that the streamline of DSP shows a regular spiral shape, due to the

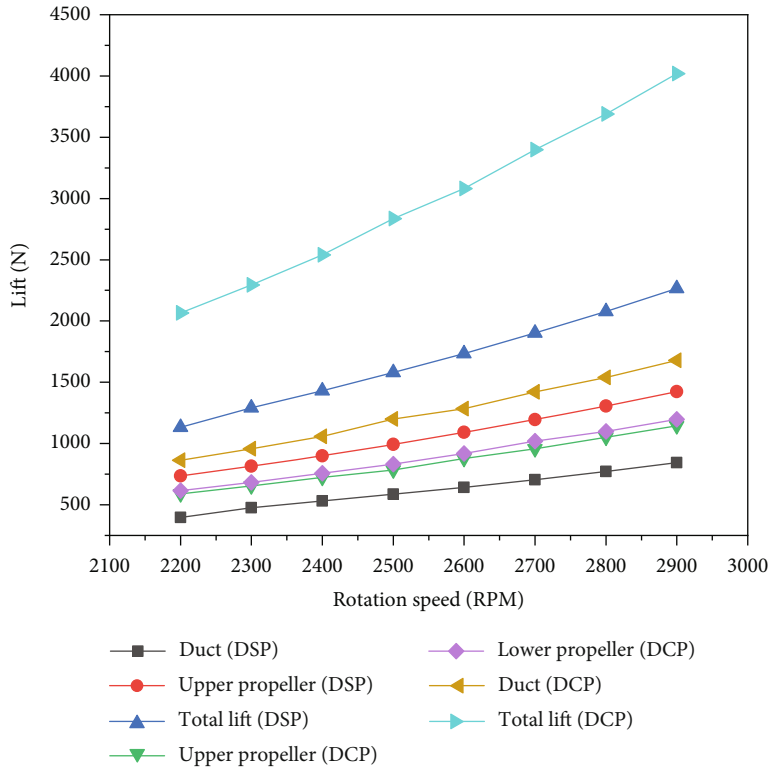

(a) Lift breakdown on each part under different rotation speed

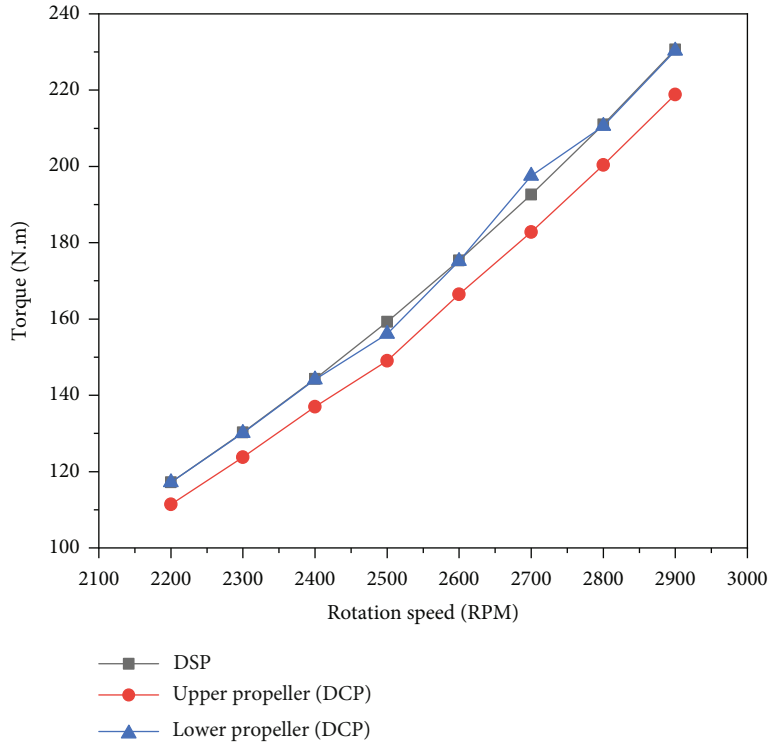

(b) Torque breakdown on each part under different rotation speed

Figure 11: Lift and torque break down on each parts of DCP and DSP.

existence of radical-induced velocity in the slipstream area. The DSP streamline twist is larger and more regular than that of DCP. The radical-induced velocity consumes part of the mechanical energy of the propeller, which reduces the static pressure in the slipstream area and decreases the aerodynamic efficiency of the propeller.

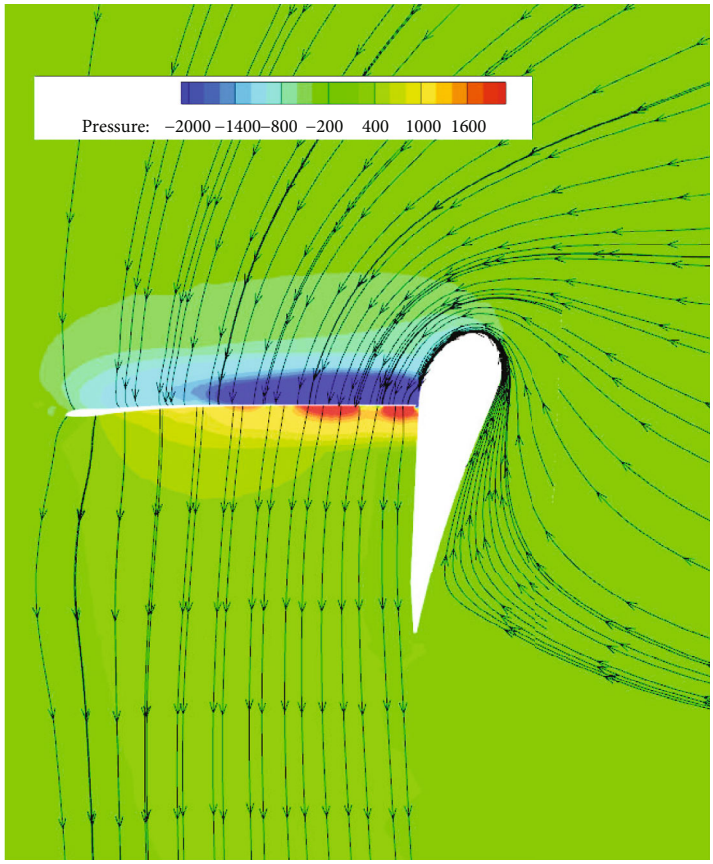

(a) Streamline diagram and pressure contour of DSP

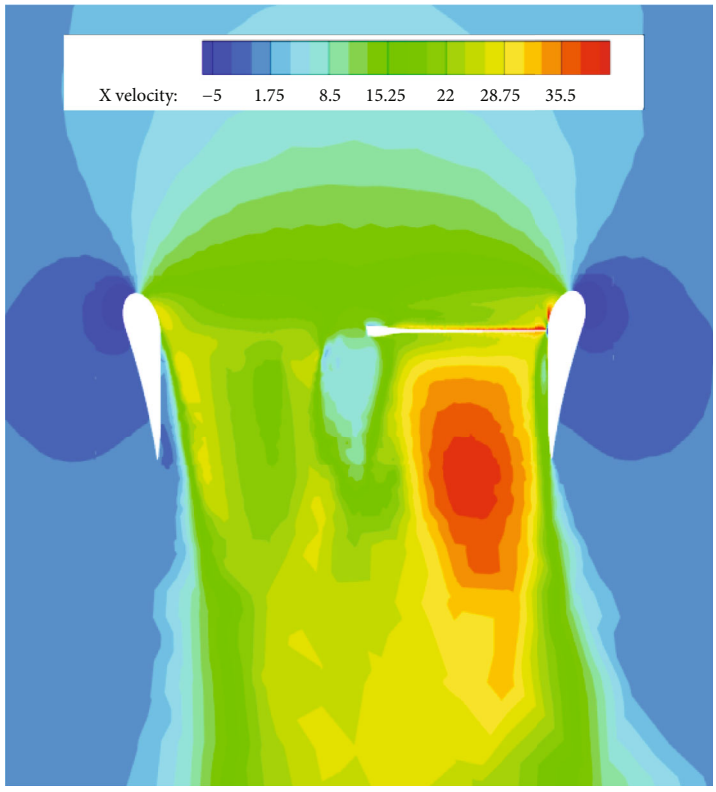

(b) Contour of the axial induced velocity of DSP

Figure 12: Streamline diagram and pressure velocity contour of DSP.

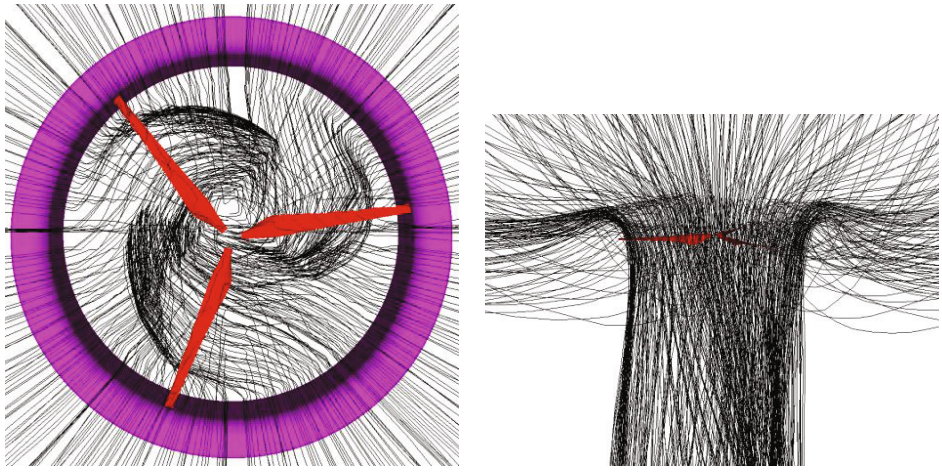

(a) Top view of DSP (b) Main view of DSP

Figure 13: Streamline diagram.

4. Conclusions

This paper aims to investigate the aerodynamic features of DCP in hovering and proposes a numerical simulation approach based on slip grid capable of simulating the DCP's flow field. The CFD calculations were compared with experimental results to validate the accuracy and reliability of the proposed CFD method. The aerodynamic characteristics of DCP were compared to those of FCP and DSP to reveal the interaction mechanism of unsteady flow between the duct and propellers. The following conclusions can be made.

(1) Compared with FCP, the duct decreases the lift of the upper and lower propellers, and the lift loss of the upper propeller is higher than that of the lower. In addition, the duct generates additional lift that offsets the propeller lift loss, resulting in the total lift 1.39 times that of the FCP. With similar power consumed by DCP and FCP, the aerodynamic efficiency of DCP is 39% higher than that of FCP

(2) Duct improves the aerodynamic efficiency of FSP, and the aerodynamic mechanisms are as follows. Firstly, the duct changes the propeller tip winding characteristics, significantly reducing tip vortex and increasing the lift-to-drag ratio of blade tip. Secondly, the duct decreases the radical-induced velocity in the slipstream area, reducing the static pressure loss. Thirdly, the wake contraction is suppressed, reducing the axial induced velocity and induced power

(3) The duct lift factor of DCP is larger than that of DSP, where the duct lift factor of DCP is 41.7% and that of DSP is 37.1%. The total lift generated by DCP is 1.77 times that of DSP, but its total aerodynamic efficiency is 91.08% that of DSP

Abbreviations

eVTOL: Electric vertical takeoff and landing
DCP: Ducted coaxial propeller
FCP: Free coaxial propeller
DSP: Ducted single propeller
ESC: Electronic stability controller.

Data Availability

The data used to support the findings of this study are available from the corresponding author upon request.

Conflicts of Interest

The authors declare that they have no conflicts of interest.

Acknowledgments

This study was supported by the Postgraduate Research and Practice Innovation Plan of Jiangsu (KYCX20_0217) and thanks to a project funded by the Priority Academic Program Development of Jiangsu Higher Education Institutions.

References

[1] C. Pornet and A. T. Isikveren, "Conceptual design of hybrid-electric transport aircraft," *Progress in Aerospace Sciences*, vol. 79, pp. 114–135, 2015.

[2] N. Polaczyk, E. Trombino, P. Wei, and M. Mitici, "A review of current technology and research in urban on-demand air mobility applications," in *Proceedings of the Vertical Flight Society's 6th Annual Electric VTOL Symposium*, pp. 333–343, Mesa, AZ, USA, 2019.

[3] A. Zanotti and D. Algarotti, "Aerodynamic interaction between tandem overlapping propellers in eVTOL airplane mode flight condition," *Aerospace Science and Technology*, vol. 124, article 107518, 2022.

[4] V. Hrishikeshavan, J. Black, and I. Chopra, "Design and performance of a quad-shrouded rotor micro air vehicle," *Journal of Aircraft*, vol. 51, no. 3, pp. 779–791, 2014.

[5] R. C. Rubio, P. V. Diaz, and S. Yoon, "High-fidelity computational analysis of ducted and coaxial rotors for urban air mobility," in *Proceedings of the Vertical Flight Society 75th Annual Forum*, pp. 1–9, Philadelphia, PA, USA, 2019.

[6] R. B. Gray and T. Wright, "Determination of the design parameters for optimum heavily loaded ducted fans," in *VTOL Research, Design, and Operations Meeting*, p. 222, Atlanta, GA, USA, 1969.

[7] A. H. Sacks and J. A. Burnell, "Ducted propellers–a critical review of the state of the art," *Progress in Aerospace Sciences*, vol. 3, no. C, pp. 85–135, 1962.

[8] A. Akturk and C. Camci, "Experimental and computational assessment of a ducted-fan rotor flow model," *Journal of Aircraft*, vol. 49, no. 3, pp. 885–897, 2012.

[9] A. Akturk and C. Camci, "Tip clearance investigation of a ducted fan used in VTOL unmanned aerial vehicles—part I: baseline experiments and computational validation," *Journal of Turbomachinery*, vol. 136, no. 2, pp. 94–113, 2014.

[10] S. Deng, S. Wang, and Z. Zhang, "Aerodynamic performance assessment of a ducted fan UAV for VTOL applications," *Aerospace Science and Technology*, vol. 103, no. 1, article 105895, 2020.

[11] G. Bernardini, F. Centracchio, M. Gennaretti et al., "Numerical characterisation of the aeroacoustic signature of propeller arrays for distributed electric propulsion," *Applied Sciences*, vol. 10, no. 8, p. 2643, 2020.

[12] C. Poggi, M. Rossetti, J. Serafini, G. Bernardini, M. Gennaretti, and U. Iemma, "Neural network meta–modelling for an efficient prediction of propeller array acoustic signature," *Aerospace Science and Technology*, vol. 130, article 107910, 2022.

[13] H. Cai, Z. Wu, S. Deng, and T. Xiao, "Numerical prediction of unsteady aerodynamics for a ducted fan micro air vehicle," *Proceedings of the Institution of Mechanical Engineers, Part G: Journal of Aerospace Engineering*, vol. 229, no. 1, pp. 87–95, 2015.

[14] H. Cai, Z. Zhang, and S. Deng, "Numerical prediction of unsteady aerodynamics of a ducted fan unmanned aerial vehicle in hovering," *Aerospace*, vol. 9, no. 6, p. 318, 2022.

[15] M. Biava and G. N. Barakos, "Optimisation of ducted propellers for hybrid air vehicles using high-fidelity CFD," *Aeronautical Journal*, vol. 120, no. 1232, pp. 1632–1657, 2016.

[16] J. Qing, Y. Hu, Y. Wang, Z. Liu, X. Fu, and W. Liu, "Kriging assisted integrated rotor-duct optimization for ducted fan in hover," in *AIAA Scitech 2019 Forum*, pp. 1–17, San Diego, CA, USA, 2019.

[17] R. Singh, B. Jimenez, and M. Avera, "Investigation of aerodynamic interactions in ducted rotor systems," in *The AHS 70th Annual Forum*, pp. 2951–2957, Montréal, Québec, USA, 2014.

[18] D. Shukla and N. Komerath, "Rotor–duct aerodynamic and acoustic interactions at low Reynolds number," *Experiments in Fluids*, vol. 60, no. 1, pp. 1–14, 2019.

[19] M. R. Colman, S. Suzuki, and D. Kubo, "Wind tunnel test results and performance prediction for a ducted fan with collective and cyclic pitch actuation for VTOL with efficient cruise," in *AIAA Atmospheric Flight Mechanics Conference*, p. 6379, Portland, Oregon, 2011.

[20] J. Wang, R. Chen, and J. Lu, "Experimental and numerical studies on the effect of airflow separation suppression on aerodynamic performance of a ducted coaxial propeller in hovering," *Aerospace*, vol. 10, no. 1, pp. 11–11, 2023.

[21] N. Roh, S. Oh, and D. Park, "Aerodynamic characteristics of helicopter with ducted fan tail rotor in hover under low-speed crosswind," *International Journal of Aerospace Engineering*, vol. 2020, Article ID 7059209, 14 pages, 2020.

[22] C. Wang, M. Q. Huang, S. Ma, H. W. Wang, and M. Tang, "Main rotor wake interference effects on tail rotor thrust in crosswind," *International Journal of Aerospace Engineering*, vol. 2021, Article ID 9994115, 13 pages, 2021.

[23] F. R. Menter, "Zonal two equation κ-ω turbulence models for aerodynamic flows," in *23rd Fluid Dynamics, Plasmadynamics, and Lasers Conference*, p. 2906, Orlando, FL, USA, 1993.

[24] J. Blazek, "Computational fluid dynamics: principles and applications," *Computational Fluid Dynamics Principles & Applications*, vol. 55, no. 2, pp. 30–54, 2001.

[25] P. L. Roe, "Approximate Riemann solvers, parameter vectors, and difference schemes," *Journal of Computational Physics*, vol. 135, no. 2, pp. 250–258, 1997.

[26] H. Luo, J. D. Baum, and R. Löhner, "An accurate, fast, matrix-free implicit method for computing unsteady flows on unstructured grids," *Computers & Fluids*, vol. 30, no. 2, pp. 137–159, 2001.

[27] Y. J. Choi, S. Wie, and S. Chae, "A study on hover performance of ducted fans for an unmanned VTOL aircraft," *International Journal of Aerospace Engineering*, vol. 2022, Article ID 4045778, 10 pages, 2022.

[28] M. Shur, M. Strelets, A. Travin et al., "Experimental/numerical study of ducted-fan noise: effect of duct inlet shape," *AIAA Journal*, vol. 56, no. 3, pp. 979–996, 2018.